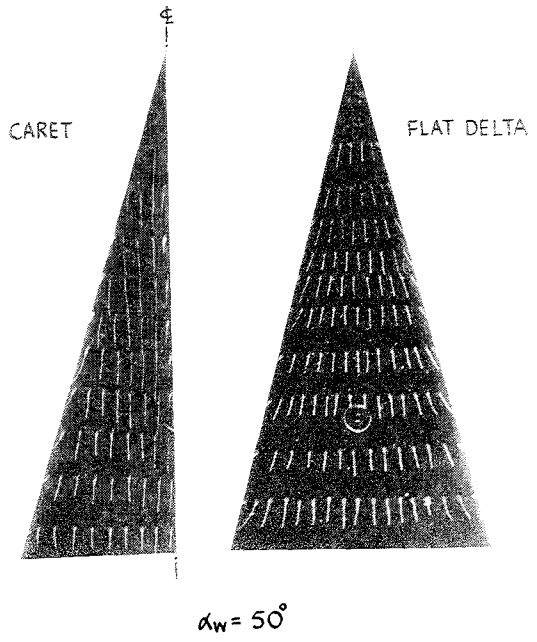


**Fig. 3 Comparison of windward surface flow patterns on caret wing and flat delta.**

nel at Imperial College, London, fitted with a contoured $M = 12$ nozzle, at a freestream unit Reynolds number of $0.15 \times 10^6$/in. (model Reynolds number based on center chord length $0.75 \times 10^6$). The 3-component strain-gage sting balance used for these measurements has been fully described in Ref. 1. The models were sting supported on the lee side, with a preset angle of 30° between the windward surface (or windward corner in case of caret wing) and the balance axis. The caret wing was designed to support a two-dimensional shock at $\alpha_w = 34°$ (incidence measured with respect to windward corner).

The normal force data for the two models, obtained from balance axial and normal force results are shown in Fig. 1. The caret wing develops a consistently higher normal force coefficient in comparison with the flat delta throughout the range of incidence. The two-dimensional shock theory predicts the caret wing characteristics quite well right up to the theoretical shock detachment, well beyond the design point. The measurements at higher incidence angles appear to continue to follow the two-dimensional shock trend. On the other hand, the flat delta normal force approaches the simple Newtonian value at the highest incidence of the test.

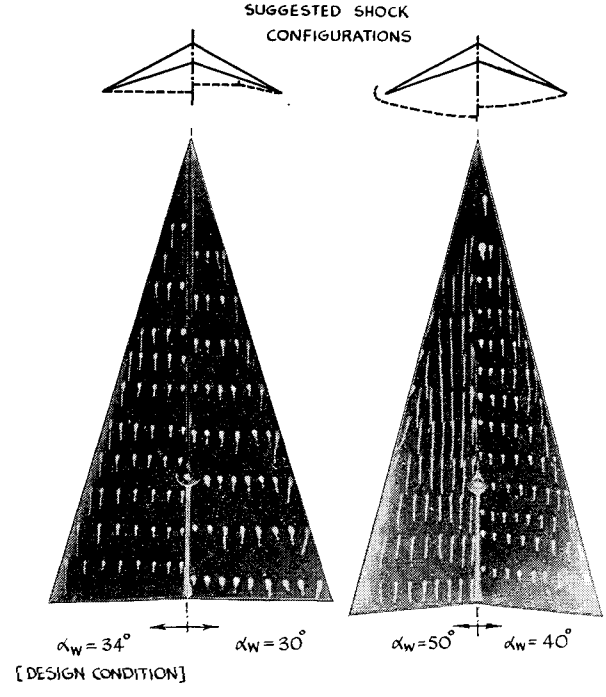


**Fig. 4 Composite photographs of windward surface flow patterns on the caret wing.**

The difference in terms of maximum lift coefficient (Fig. 2) is nearly 40% in favor of the caret wing under the conditions of the present tests. It may be noted that the lift/drag ratio coincides with $\cot\alpha_w$, indicating that at these high incidence angles the aerodynamic load is essentially generated by the windward surface pressure on both the wings, the axial force due to skin friction and base pressure being negligible.

Surface flow visualization on the windward surfaces at the maximum incidence of the test ($\alpha_w = 50°$, Fig. 3) reveals that the flow was essentially "contained" under the caret wing, the flow spillage being limited to a very narrow strip along the leading edges. With the flat delta, however, three-dimensional flow extends over a considerable portion of the pressure surface.

Additional oil flow results for the caret wing at different incidence angles (Fig. 4) show some interesting features. At design incidence, an essentially "two-dimensional" flow was achieved (i.e., flow parallel to the center chord). Regions of relatively high shear along the leading edge and low shear in the corner (along center chord) can be identified. At 30° incidence (i.e., only 4° below the design value) the flow entering the leading edge is directed inwards, a change to parallel flow apparently occurring along a conical ray close to the leading edge. As the incidence increases above the design value, coincident with the detachment of the leading-edge shock and the appearance of an attachment (or stagnation) line under the leading edge, the flow spills over the edge as seen for $\alpha_w = 50°$. These changes are, however, limited to the leading-edge zone, the flow over most of the windward surface of the caret wing remaining substantially "two-dimensional" over a large range of incidence. These flow visualization results serve to explain the superiority of the caret wing force characteristics over the flat delta.

### References

[1] Opatowski, T., "An Experimental Study of the Flow Around and the Forces Developed by Hypersonic Lifting Vehicles," Ph.D. thesis, Sept. 1967, London University; also Repts. 30,997 and 31,278, Aeronautical Research Council, United Kingdom.

[2] Townend, L. H., "Some Aerodynamic Considerations of Lifting Re-entry Vehicles," Rept. 32,104, May 1970, Aeronautical Research Council, United Kingdom.

# A Simplification Technique for Thermal Radiation in Gray Enclosures

JOHN J. CHAPTER*
*Martin Marietta Corporation, Denver, Colo.*

### Nomenclature

$A_i$ = area of $i$
$F_{i-j}$ = over-all radiant interchange factor from $i$ to $j$
$G_{m-i}$ = over-all thermal conductance from node $m$ to $i$
$i$ = $i$th enclosure node
$m$ = node number
$M_i$ = number of nonenclosure nodes coupled to $i$

Received July 23, 1970.

* Senior Engineer, Skylab Program Apollo Telescope Mount (ATM) Unit. Member AIAA.

$N$ = number of nodes in thermal network radiation enclosure
$P_i$ = number of primary radiation couplings for node $i$
$q_i$ = applied heat load to node $i$
$T$ = absolute temperature
$T_i, T_i'$ = exact and approximate temperature of ith enclosure node
$\gamma$ = fraction of sum of enclosure node radiators that will be left intact
$\epsilon$ = emissivity
$\sigma$ = Stefan-Boltzmann constant

***Subscripts***

ERN = Effective Radiation steady-state Node
$j$ = enclosure nodes
$k$ = primary radiators
$l$ = secondary radiators

NODAL thermal analysis techniques are used extensively in support of spacecraft thermal design. Thermal radiation is often the predominant mode of heat transfer in vehicle cabins, equipment bays, and tank enclosures. Radiation modeling is cumbersome because of interactions due to thermal reflection, possibly resulting in large numbers of radiative couplings.[1] Recently, computer programs have been developed that apply the methods of Hottel and Gebhart to calculate the complete enclosure radiant interchange matrix.[2,3] The impetus to develop the new generation computer program has been because previous approximate methods did not have the capability to include reflection effects due to moderate and low emissivity ($\epsilon < 0.5$) nodes. This increased analytical capability has been tempered by increased radiation matrix size that must be accommodated for when using thermal analyzer programs. A typical 150-node enclosure would potentially contain 11,175 radiative paths, thus the definition of the radiation mode becomes prohibitive for contemporary computers. Computer run time may approach real mission time. Integrated thermal models for complete spacecraft are often desirable and the requirement for radiation simplification techniques is obvious. This Note presents a new simplification technique that is general and reduces the complexity of radiation enclosures.

The usual method to reduce the number of radiative couplings has been limited to neglect of small valued couplings. A technique has been developed where a steady-state node referred to as an enclosure, Effective Radiation Node (ERN), is defined. Depending on desired accuracy, a fraction of the total radiative paths of each node is left intact with the remaining summed, and coupled to the enclosure ERN. The ERN method does not neglect small radiative couplings because the total emissive power for each node remains equal to that of the original matrix. The Radiation Condenser (RC) computer program makes the application of the ERN technique for the CINDA thermal analyzer practical.[4] The program is being used in conjunction with thermal models of the NASA Skylab cluster and ATM vehicles.

## Effective Radiation Node Technique

Consider an $N$ node radiative enclosure that forms a section of a complex thermal network. The $i$th enclosure node is coupled to $M_i$ arbitrary network nodes $m$, with conductors $G_{m-i}$. The node temperature is a function of the radiation to other enclosure nodes, couplings to network nodes (radiation, conduction, convection), and applied heat loads. The steady-state temperature for node $i$ is

$$T_i = \left[\left(\sum_{j=1}^{N} \sigma A_i F_{i-j} T_j^4 + \sum_{m=1}^{Mi} G_{m-i} T_m + q_i\right) \Big/ \left(\sum_{j=1}^{N} \sigma A_i F_{i-j} + \sum_{m=1}^{Mi} G_{m-i}\right)\right]^{1/4} \quad (1)$$

Assume that the enclosure radiative couplings (radiators) of the $i$th node have been divided into $P_i$ primary and $N - P_i$ secondary terms. The node radiators can then be written

$$\sum_{j=1}^{N} \sigma A_i F_{i-j} = \sum_{k=1}^{Pi} \sigma A_i F_{i-k} + \sum_{l=Pi+1}^{N} \sigma A_i F_{i-l} \quad (2)$$

The number of radiators is reduced by replacing the secondary coupling summation with a single term coupled to an ERN. For the $i$th node

$$\sum_{l=Pi+1}^{N} \sigma A_i F_{i-l} T_l^4 = \left[\sum_{l=Pi+1}^{N} \sigma A_i F_{i-l}\right] T_{\mathrm{ERN}i}^4 \quad (3)$$

Ideally, each enclosure node should have its own ERN which would result in zero error. However, calculation of the individual $T_{\mathrm{ERN}i}$ requires all secondary terms and results in no reduction. A single overall enclosure ERN temperature is established as an approximation for $T_{\mathrm{ERN}i}$. The ERN temperature is calculated by the thermal analyzer program as a steady-state node with a fourth-power weighted average using node secondary radiator sums:

$$T_{\mathrm{ERN}} = \left[\sum_{i=1}^{N}\sum_{l=Pi+1}^{N} \sigma A_i F_{i-l} T_i^4 \Big/ \sum_{i=1}^{N}\sum_{l=Pi+1}^{N} \sigma A_i F_{i-l}\right]^{1/4} \quad (4)$$

The $i$th node temperature can be rewritten from Eq. 1 using the enclosure ERN as

$$T_i' = \left\{\left(\sum_{k=1}^{Pi} \sigma A_i F_{i-k} T_k^4 + \left[\sum_{l=Pi+1}^{N} \sigma A_i F_{i-l}\right] T_{\mathrm{ERN}}^4 + \sum_{m=1}^{Mi} G_{m-i} T_m^4 + q_i\right) \Big/ \left(\sum_{j=1}^{N} \sigma A_i F_{i-j} + \sum_{m=1}^{Mi} G_{m-i}\right)\right\}^{1/4} \quad (5)$$

The error in the approximate $i$th node temperature $T_i'$ is a complex function of the relative order of magnitude of Eq. (5) terms, the percentage of secondary radiators, and the temperature band of the enclosure nodes. For many problems the error has been found to be negligible and empirical guidelines have been determined.

## ERN Computer Program

The generation of ERN radiators from the radiant interchange matrix has been computerized with the RC program. The program technique is simple and can be adapted to any radiant interchange computer program.

A simplified flow diagram for RC program logic is given in Fig. 1. Node radiators are arranged by the program in decreasing order of the radiator ($A_i F_{i-j}$) value. The analyst assigns the primary radiation fraction $\gamma$, and the program operates on each node selecting the largest remaining radiator values. This procedure is terminated when the sum of selected terms is greater than the fraction $\gamma$ of each node's total radiators. Reverse direction radiators are flagged and the remaining radiators for each node are summed and coupled to the ERN. Since the error is a function of the enclosure temperature band, the ERN approximation can be improved if nodes that deviate significantly in temperature from the average enclosure temperature are not coupled to the ERN. These analyst-defined nodes are referred to as special nodes in the RC program.

The RC program and ERN application have been verified by comparison analysis using the CINDA thermal analyzer with typical Skylab crew and equipment enclosures. A typical spacecraft equipment enclosure of the Skylab ATM experiment package has been selected for verification analysis. The ATM octagonal structure serves as a support for a cylindrical enclosure referred to as the canister. One of the four enclosures of the canister network contains a 135 node radiation enclosure within a 235 node network. Canister solar telescopes and equipment are radiatively cooled by sur-

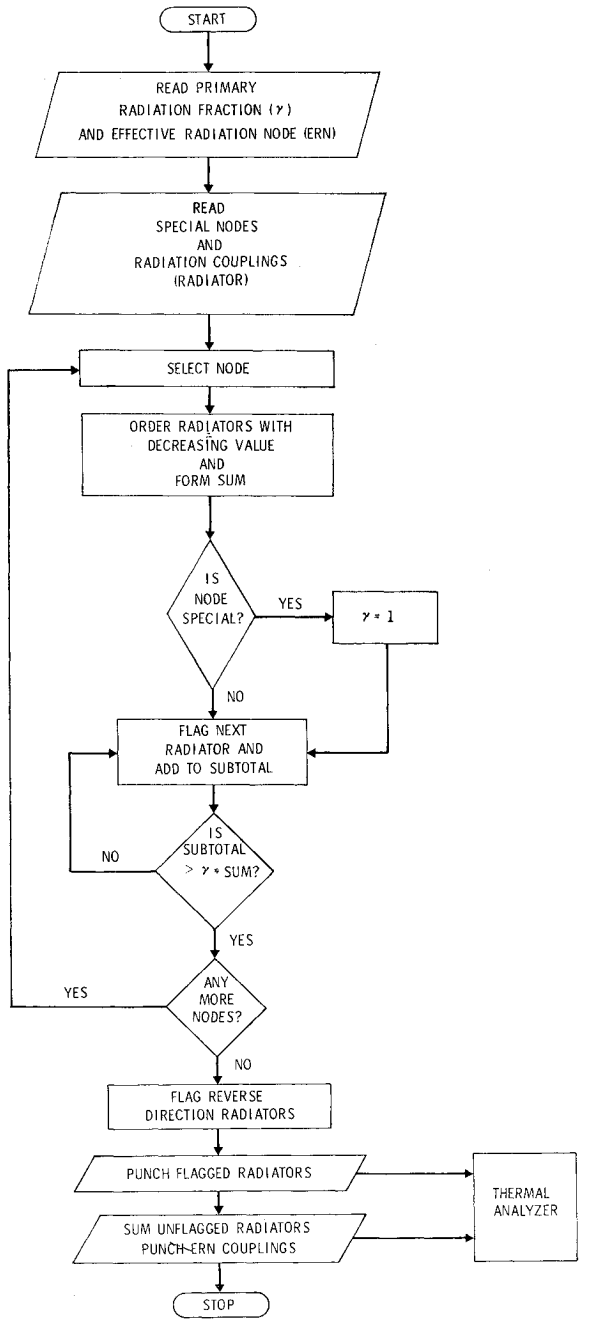


**Fig. 1 Simplified flow diagram for the RC program.**

rounding coldplates. These nodes were defined as RC special nodes and their couplings were left intact. Application of the RC program reduced the number of enclosure radiators from 2450 to 620, with a $\gamma$ of 0.7. Comparative thermal analysis showed that the maximum temperature error in using the ERN node was 0.5°F. Similar results have been obtained for other network enclosures including the Skylab cluster vehicle compartments.

For a constant $\gamma$, experience has shown that the greatest percentage reduction in radiators is for large enclosures (greater than 75 nodes) with significant shadowing and low emittance surfaces. The smallest radiator reduction is for enclosures with a low number of nodes (less than 30) with symmetrical geometry. A $\gamma$ value of 0.7 has been found to be a good compromise value that results in significant reduction in couplings with acceptable error.

The ERN technique is general and can be used to reduce the number of radiative paths required to model typical spacecraft enclosures. The percentage reduction in enclosure radiators and subsequent network error is controlled by the analyst selection of a $\gamma$ value consistent with known accuracy of problem parameters (enclosure geometry, surface properties).

### References

[1] Werner, J. B. and Starret, P. S., "Experiment Heat Transfer Correlation of a Complex Model," *Journal of Spacecraft and Rockets*, Vol. 5, No. 3, March 1968, pp. 247–252.

[2] Wiebelt, J. A., *Engineering Radiation Heat Transfer*, Holt, Rinehart and Winston, New York, 1966.

[3] Holmstead, G. M., "Martin Thermal Radiation Analyzer Program," Inter-Department Communication, Aug. 1969, Martin Marietta Corp., Denver, Colo.

[4] Connor, R. J., Kannady, R. E., Jr., and Alamanza, J. E., "Adaptation of Chrysler Improved Numerical Differencing Analyzer to CDC 6000 Series Computers," Engineering Dept. Technical Manual M-68-22, Nov. 1969, Martin Marietta Corp., Denver, Colo.

# Optimization of Stored Pressurant Supply for Liquid Propulsion Systems

GILBERT F. PASLEY*
*Hughes Aircraft Company, El Segundo, Calif.*

### Nomenclature

| | | |
|---|---|---|
| $A$ | = | surface area |
| $C$ | = | specific heat |
| $c_v$ | = | specific heat, constant volume |
| $g$ | = | acceleration of gravity |
| $Gr$ | = | Grashof number |
| $H,h$ | = | heat-transfer coefficient and enthalpy, respectively |
| $M,m$ | = | tank and fluid masses, respectively |
| $Nu$ | = | Nusselt number |
| $p$ | = | pressure |
| $Pr$ | = | Prandtl number |
| $Q$ | = | heat content |
| $R$ | = | pressurant gas constant |
| $\rho$ | = | fluid density |
| $T,t$ | = | temperature and time, respectively |
| $u$ | = | internal energy |
| $V,v$ | = | fluid velocity and specific volume, respectively |

***Subscripts***

0,1,2,3 = pressurant tank, regulator inlet, propellant tank ullage, and propellant feed line locations, respectively

### Introduction

A THERMODYNAMIC study of a particular pressurization system leads to a set of complex differential equations which analysts have attempted to simplify by approximating the actual thermodynamic processes.[1,2] These approximations allow a closed-form solution but introduce errors too severe for final design purposes. This Note describes a mathematical model of the pressurization system used on the Surveyor lunar-landing spacecraft that was formulated with a minimum of simplifying assumptions. The predicted performance is compared with test data.

### Discussion

The Surveyor spacecraft was designed and built by Hughes Aircraft Company under the direction of the California Insti-

Received June 4, 1970; revision received August 28, 1970.

* Member of Technical Staff, Space Systems Division. Member AIAA.